https://doi.org/10.5194/wes-2023-163
Preprint. Discussion started: 30 January 2024

eawe european academy of wind energy
Open Access WIND ENERGY SCIENCE DISCUSSIONS

Load case selection for finite element simulations of wind turbine pitch bearings and hubs

Matthias Stammler[1] and Florian Schleich[1]

[1]Large Bearing Laboratory, Fraunhofer Institute for Wind Energy Systems IWES, Hamburg, 21029, Germany

Correspondence: Matthias Stammler (matthias.stammler@iwes.fraunhofer.de)

Abstract. Finite element simulations of large rolling bearings and structural parts are an indispensable tool in the design of wind turbines. Unlike simpler structures or smaller bearings in rigid environments where analytical formulas suffice, wind turbine components require a more comprehensive approach. This is because analytical formulas often fall short in predicting load distributions and stresses, leading to inadequate designs. However, due to the size of the finite element models and operational loads involved, it's necessary to strike a balance between achieving realistic results and keeping computational times manageable. This study focuses on the selection of load cases for simulations of pitch bearings and hubs of wind turbines. The models for these contain the hub, the pitch bearings, the inner parts of three blades, and any necessary interfaces parts. The simulation results allow the calculation of static and fatigue strength. Given the complexity of the problem, with each rotor blade having six degrees of freedom, five types of loads, and the pitch angle, the potential combinations of loads would result in an unmanageably high number of required simulations. The present work exploits relationships between load components and the rotor position to reduce the number of load cases needed for fatigue calculations. The IWT 7.5-164 reference turbine and three commercial turbines serve as the basis for case studies which include bin counts and exemplary finite element simulations. The blade's azimuth angle and bending moments of one blade allow determining the loads at all three blade roots with a reasonable degree of confidence.

1 Introduction

Pitch bearings of wind turbines are slewing bearings which connect each rotor blade with the rotor hub (Hau, 2017). There are several commercially available design types for these bearings, as listed in (Stammler, 2020). Bearings can fail for various reasons as described in ISO 15243 (ISO, 2017). Rolling contact fatigue and structural fatigue of the rings are among those and are driven by stress cycles.

Hubs are the structural centerpiece of wind turbine rotors, providing the linkage between the three blades and the turbine's drive train. Similar to the pitch bearing ring, the structural integrity of hubs is influenced by stress cycles, which drive fatigue (Hau, 2017).

Aero-elastic simulations of wind turbines provide the load time-series at various positions, such as the rotor blade roots (Burton et al., 2011; Hau, 2017). In order to assess the lifespan of individual components, it is necessary to establish a relation-

https://doi.org/10.5194/wes-2023-163
Preprint. Discussion started: 30 January 2024

eawe european academy of wind energy
Open Access WIND ENERGY SCIENCE DISCUSSIONS

ship between the applied loads and the resulting stresses. This involves calculating the nonlinear dependencies between these variables. Finite element (FE) simulations derive these relations for each calculated load case.

In theory it is possible to use FE simulations with the loads at each discrete time step of the input data. This approach would yield time series data of stresses, which could then be utilized for analytical fatigue calculations. Doing so is not possible within reasonable computing times and a reduction of load cases for the simulations is therefore necessary.

Aside from the definition of load cases, the selection of a model type is another crucial aspect for a FE simulation. This study covers full rotors with three blades. The load and stress distributions of pitch bearings and hubs are influenced by the loads the three rotor blades transfer to their roots. It is assumed that the stress distribution in one pitch bearing is influenced by the loads of the other pitch bearings.

(Chen and Wen, 2012) simulated a double-row four-point contact ball bearing that is used as pitch bearing in a 1.5 MW wind turbine. They used a model with three rotor blade roots but did not elucidate on the selection of load cases.

To the best knowledge of the authors, the only approaches for load case selection published in literature are limited to the determination of load cases for one blade root, i.e. one pitch bearing:

- Characterise and simplify the input load time series by means of rainflow counts and use the reduced data to define load cases for the FE. Use the results, which again have the form of rainflow count results, to calculate fatigue.
- Use the extreme operating loads. Evenly spread load steps in between those and calculate the results for these load cases. Interpolate between the results to obtain stress time-series and apply rainflow counts to calculate fatigue.

Both approaches will result in inaccurate results in comparison to FE simulations of each time step of the input data. The extent of the inaccuracies depends on the number of load cases simulated and the turbine configuration.

Becker et al. (2017) describe a process as per the first of the abovementioned approaches where the input load time series are first processed into rainflow counts which then give the load cases for the FE simulations. To account for the complex behavior of large bearings, the bearings circumference is split into several sections, for each of which the rainflow counts are done.

Stammler et al. (2018) did 126 simulations with a rotor of a 3 MW turbine with variations of pitch angles and bending moments. They evaluated the load distribution in one pitch bearing, kept the pitch angles of the other bearings constant and the loads at the other bearings at one third of the loads of the primary bearing. They did not elucidate on the reasons for the load case selection. The load distribution in the pitch bearing was shown to be dependent on the interfaces.

Menck et al. (2020) used a one-third rotor with rotational symmetric boundary conditions to reduce the computational effort in comparison to a full rotor. The ran 358 simulations on this model and varied the pitch angle and the resulting bending moment and its angle as per the second approach. With a regression of the resultant rolling body loads they obtained time series of rolling body loads and calculated the fatigue life of the bearing raceways.

Becker and Jorgensen (2023) stated the need of full rotor simulations for pitch-bearing damage modes which are driven by edgewise loads of the blades.

Figures 1 and 2 summarize the two published approaches as flow charts. Figure 1 depicts the approach by Becker et al. (2017). The input load time series (upper left box) are processed by rainflow counts of the loads of an arbitrarily selected blade

https://doi.org/10.5194/wes-2023-163
Preprint. Discussion started: 30 January 2024

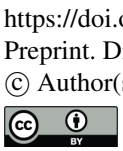

eawe european academy of wind energy
Open Access WIND ENERGY SCIENCE DISCUSSIONS

Figure 1. Flowchart of load case selection with preceding rainflow count

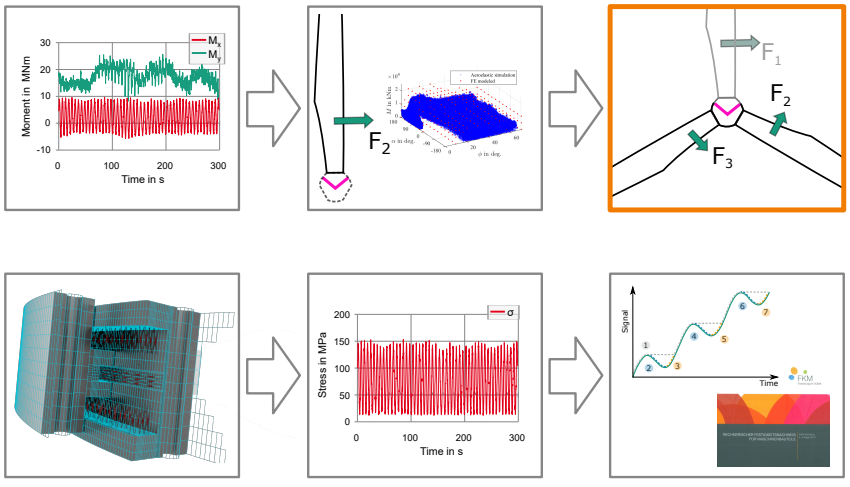

Figure 2. Flowchart of load case selection with preceding interpolation and stress-time series creation

one (upper center box). These are then used for finite element simulations of the pitch bearings and their interfaces (lower left box). As the load cases already are given in form of rainflow counts, the FE-results can be used directly for fatigue calculations. The FKM guideline contains methods for such calculations (lower center box, FKM (2012). The selection of the loads of the other blades (upper right box in orange) is not explained in the publications.

Figure 2 depicts the approach by Stammler et al. (2018) and Menck et al. (2020). The input loads (upper left box) are processed evaluated to obtain the ranges of each signal. In between the extreme values, a grid of load cases is created (upper

https://doi.org/10.5194/wes-2023-163
Preprint. Discussion started: 30 January 2024

eawe european academy of wind energy
Open Access WIND ENERGY SCIENCE DISCUSSIONS

center box). These are then used for finite element simulations of the pitch bearings and their interfaces (lower left box). The results need additional postprocessing by interpolation to obtain stress-time series (lower center box). A rainflow count of these time series is then used for fatigue calculations (lower right box). The selection of the loads of the other blades (upper right box in orange) is either omitted or not explained in detail in the publications.

To the authors' knowledge, there is a notable gap in the existing literature regarding a comprehensive exploration of load case selection specifically for pitch bearing simulations involving three rotor blades, highlighted by the orange boxes in Figure 1 and 2 flow charts. Furthermore, there appears to be a lack of published works addressing load case selection for rotor hubs.

The central inquiry driving this study is the extent to which the individual load components on each rotor blade are interconnected or affected by other signals. In essence, this research extends beyond the existing approaches by shedding light on how the loads of an arbitrarily selected blade are correlated with and influenced by the loads of the other blades.

The remainder of this article begins with Section 2, which introduces definitions for the following sections, the necessary data input, and the methods which are applied to determine dependencies. The data input for the case studies includes aeroelastic simulation time series of the IWT7.5-164 reference turbine and three commercial turbines. Section 3 covers the results of the case studies and shows which relationships are useful for the load case selection. The final discussion and conclusions then summarizes the findings of this work.

2 Definitions and methods

2.1 Coordinate systems

Pitch bearing loads in this study use the coordinate system shown in Figure 3 with the exception of the pitch angle θ, which is positive in mathematically negative sense. This convention is industry standard, and most turbine simulation time series follow it. Although the coordinate system does not rotate with the pitch angle, the term flapwise bending moment refers to $M_{y,\mathrm{B}}$ and the term edgewise bending moment to $M_{x,\mathrm{B}}$ in the following. Strictly speaking, $M_{y,\mathrm{B}}$ is only a pure flapwise moment if the pitch is at $0°$. Flapwise bending moments are the result of wind thrust, whereas edgewise bending moments are mostly dominated by gravitational forces.

Hub center loads and blade azimuth angle in this study use the coordinate system shown in Figure 4.

The blade azimuth angle $\Phi_{\mathrm{r,B}}$ is defined in Figure 5. Note that the $0°$ position is arbitrarily chosen. As long as it is consistent throughout the data set, any other position can serve as $0°$.

The three blades have the arbitrarily chosen numbers one, two, and three which are consistent throughout the simulation data set. The numbers increase clockwise seen from the incoming wind direction. $\Phi_{\mathrm{r,B}}$ refers to blade one. Blade one is also called primary blade in the following, blade two and three secondary blades.

https://doi.org/10.5194/wes-2023-163
Preprint. Discussion started: 30 January 2024

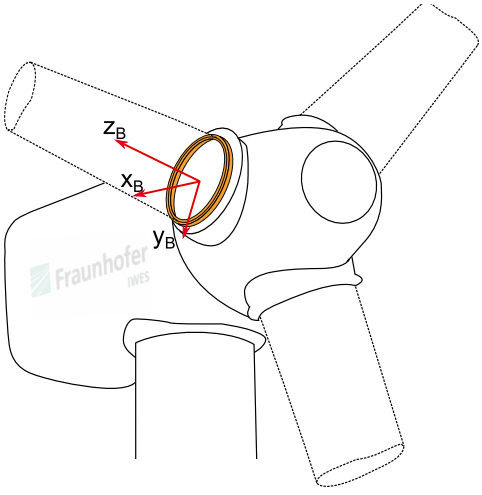

Figure 3. Pitch bearing coordinate system (fixed to rotor hub) (Stammler, 2020)

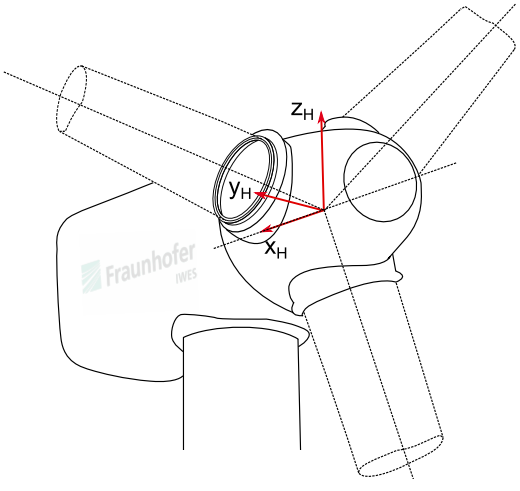

Figure 4. Hub coordinate system (fixed to turbine nacelle)

2.2 Input data and signal selection

Becker et al. (2017); Stammler et al. (2018); Menck et al. (2020); Becker and Jorgensen (2023) all use the edgewise and flapwise bending moments $M_{x,\mathrm{B}}$ and $M_{y,\mathrm{B}}$ to describe the load cases of one pitch bearing. The use of the combined bending moments $M_{\mathrm{xy,B}}$ and their load angle β is equivalent to the use of $M_{x,\mathrm{B}}$ and $M_{y,\mathrm{B}}$. Stammler et al. (2018); Menck et al. (2020) also include the pitch angle θ.

https://doi.org/10.5194/wes-2023-163
Preprint. Discussion started: 30 January 2024

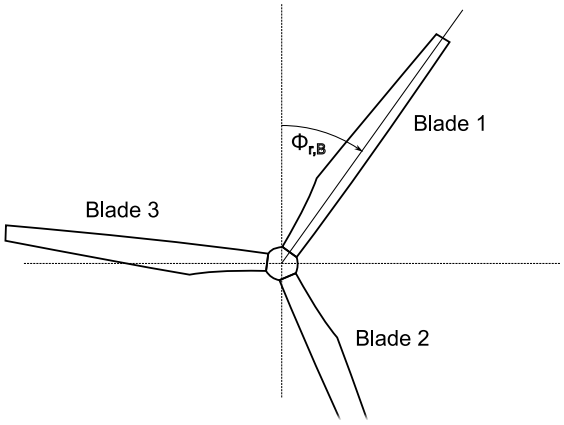

Figure 5. Blade azimuth angle $\Phi_{\mathrm{r,B}}$

The input data for simulations with three blades thus needs pitch angles θ, blade root bending moments $M_{x,\mathrm{B}}$ and $M_{y,\mathrm{B}}$, and forces $F_{x,\mathrm{B}}$, $F_{y,\mathrm{B}}$, and $F_{z,\mathrm{B}}$ for all three blades. The need for the inclusion of pitch angles bases upon the results of Stammler et al. (2018); Menck et al. (2020), who show the load distribution in a blade bearing to be dependent on the non-rotationally symmetric stiffness profile of the rotor blade.

The introduction of additional signals for the selection of load cases might render more meaningful relations between the load components. It can, however, increase the number of necessary load cases. The blade's azimuth angle $\Phi_{\mathrm{r,B}}$ and the out-of-plane rotor moment $M_{\mathrm{y,H}}$ are included as additional signals. $\Phi_{\mathrm{r,B}}$ is strongly related to the dominant 1p-component of all $M_{x,\mathrm{B}}$. The out-of plane rotor moments might help to narrow relations between the individual $M_{y,\mathrm{B}}$.

2.3 Calculation of missing time series signals

While the blade root loads of all three blades and the pitch angle of the primary blade are essential to perform the tasks laid out in the later sections of this work, the absence of other signals can be accepted as they can be derived from the aforementioned signals.

- Pitch angles of secondary blades

  Although modern turbines can have individual pitch control and differing pitch angles between the blades, it is permissible to assume same pitch angles on all three blade roots. In comparison to the larger angle changes performed by the collective pitch to control the turbine's power, the smaller travels of the individual pitch have a negligible cross-influence between the individual blade roots.

- Out-of-plane rotor moments

  The out-of-plane rotor moments $M_{\mathrm{y,H}}$ and $M_{\mathrm{z,H}}$ in a fixed frame of reference can be calculated from the individual flapwise blade root moments. This assumes $\Phi_{\mathrm{r,B}}$ as per Figure 5.

https://doi.org/10.5194/wes-2023-163
Preprint. Discussion started: 30 January 2024

eawe european academy of wind energy
Open Access WIND ENERGY SCIENCE DISCUSSIONS

$$M_{\mathrm{y,H}} = M_{\mathrm{y,B,1}} \cdot cos(\Phi_{\mathrm{r,B}}) - cos(\Phi_{\mathrm{r,B}} + \frac{2}{3}\pi)\,(M_{\mathrm{y,B,2}} + M_{\mathrm{y,B,3}}) \tag{1}$$

$$M_{\mathrm{z,H}} = M_{\mathrm{y,B,1}} \cdot sin(\Phi_{\mathrm{r,B}}) - sin(\Phi_{\mathrm{r,B}} + \frac{2}{3}\pi)\,(M_{\mathrm{y,B,2}} + M_{\mathrm{y,B,3}}) \tag{2}$$

– Blade azimuth angle

As the edgewise bending moments of the rotor blades are dominated by gravitational forces, the 1p component of $M_{x,\mathrm{B}}$ links directly to the blade azimuth angle $\Phi_{\mathrm{r,B}}$. An algorithm to obtain $\Phi_{\mathrm{r,B}}$ can be outlined as follows for each time series file:

1. Define $0°$ position for $\Phi_{\mathrm{r,B}}$, e.g. at local maximum of the first derivative of $M_{x,\mathrm{B}}$
2. Apply low pass filter to $M_{x,\mathrm{B}}$ to eliminate high frequency components
3. If necessary, calculate derivative of $M_{x,\mathrm{B}}$
4. Identify local maxima or minima
5. Check for consistency, i.e. remove extreme values in unrealistic proximity to each other from the analysis
6. For each space between extreme values: calculate linearly increasing vector ranging from $0°$ to $360°$ or 0 to 2π for the time steps from one extreme value to the next
7. Paste the resulting vector at the corresponding positions into a new $\Phi_{\mathrm{r,B,calc}}$ signal in the file
8. For a leading or trailing incomplete rotation of the rotor, use portions of the adjacent full vector

This algorithm reproduces speed changes between full rotor revolutions, but not within a revolution.It is essentially equivalent to taking the inverse sine of the 1p-component of the edgewise bending moment observed at one of the blade roots.

2.4 Bin counting and mean value evaluation

The relations between different load signals are evaluated with the help of bin counts. The relation between each time-series file duration and the period it represents of the turbine design life is expressed by multipliers. The bin results are weighed by these multipliers. One or more signals are assumed to be independent and the other signals are assumed to be dependent on them. For each bin of the independent signal(s), all assumed dependent signals are evaluated for their mean value and standard deviation. Mean value and standard deviation are weighted by the multipliers of the individual time series files. The use of the standard deviation implies the assumption of a normal distribution of the signal values around the mean value, which is not necessarily the case. Yet, it allows a good comparison between different bin counts.

https://doi.org/10.5194/wes-2023-163
Preprint. Discussion started: 30 January 2024

eawe european academy of wind energy
Open Access WIND ENERGY SCIENCE DISCUSSIONS

Table 1. Example structure of bin counting result

Independent signals			**Dependent signals**			
1st signal normalized bin range	**2nd signal normalized bin range**	**Bin count**	**3rd signal mean**	**3rd signal std**	**4th signal mean**	**4th signal std**
0 – 0.5	0 – 0.33	20	0.15	0.10	0.3	0.05
0 – 0.5	0.33 – 0.66	25	0.42	0.08	0.32	0.04
0 – 0.5	0.66 – 1	15	0.82	0.08	0.30	0.06
0.5 – 1	0 – 0.33	10	0.10	0.12	0.18	0.05
0.5 – 1	0.33 – 0.66	25	0.43	0.13	0.21	0.04
0.5 – 1	0.66 – 1	5	0.8	0.10	0.2	0.05

In case of more than one assumed independent signal, the bin counts are stacked. For each bin of the first signal, all bins of the second signal are counted. Table 1 lists an example structure of such a result for two independent signals and two dependent signals. The result values are arbitrarily chosen.

The standard deviations of dependent signals are combined by weighted means to a single standard deviation for all bins. The number of bins of the independent signals is increased until the standard deviation of dependent signals converges or until a finer resolution of bins is unreasonable.

2.5 Finite element simulations

The verification of the assumption of cross-influences between the pitch bearings and the load case selection method needs finite element simulations. This work uses bearing models as described in Graßmann et al. (2023) in a full rotor model. As the modelling approach is validated in Graßmann et al. (2023), further validation is not part of this work. The three blades are modelled according to Menck et al. (2020). A one-third rotor model (see left of Figure 6) behavior is achieved by loading all three blades with the same load. For convenience, this model is designated one-third rotor model in the following. The tangential stresses in the bore holes on the y-axis, which are mainly loaded by M_x, are taken as comparative values for different scenarios.

3 Case studies

3.1 Input data and scenario

The IWT7.5-164 is a nearshore reference wind turbine (Sevinc et al., 2014). The authors used time series data of this turbine in previous works, see (Stammler et al., 2019; Stammler, 2020). Table 2 lists the main properties of the turbine. The simulation time series, taken from Requate et al. (2020), contain all signals listed above which makes the calculation of additional signals

https://doi.org/10.5194/wes-2023-163
Preprint. Discussion started: 30 January 2024

eawe european academy of wind energy
Open Access WIND ENERGY SCIENCE DISCUSSIONS

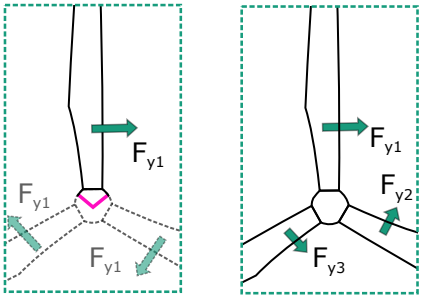

Figure 6. One-third rotor model (left) , full rotor model (right)

unnecessary. The data set comprises 156 files of the DLC1.1 with mean wind speeds from 3 to 25 m/s. Figure 7 shows the generator output power over momentary wind speed in x-direction of the hub coordinate system of Figure 4 with calculated mean values.

Table 2. Main characteristics of the IWT7.5-164, from (Stammler, 2020)

Property	Symbol	Value	Unit
Hub height	h_{hub}	119.3	m
Specific power (per swept area)	ψ_{rotor}	355	$\mathrm{W/m^2}$
Cut-in wind speed	V_{in}	3	m/s
Rated wind speed	V_{r}	11	m/s
Cut-out wind speed	V_{out}	25	m/s
Minimum rotational speed	Ω_{min}	5	rpm
Rated rotational speed	Ω_{r}	10	rpm
Rated tip speed	$V_{\mathrm{tip,r}}$	85.9	m/s

Figure 8 shows an exemplary time series of the turbine simulation data at 11 m/s mean wind speed. The top row shows the $M_{y,\mathrm{B}}$ and $F_{x,\mathrm{B}}$ of all three blades, the next row $M_{x,\mathrm{B}}$, $F_{y,\mathrm{B}}$, and $F_{z,\mathrm{B}}$ of all three blades. Signals pertaining to the same blade are displayed in the same color. Bending moments are the thick lines, forces the thin and dashed lines. The blade's azimuth angle is depicted in the third row and the two tilting moments $M_{\mathrm{y,H}}$, green, and $M_{\mathrm{z,H}}$, orange, of the rotor in the last row.

The flapwise blade moments and the rotor moment about its horizontal axis appear more stochastic than the edgewise moments and the connected forces.

Figure 9 supports the close relation of $\Phi_{\mathrm{r,B}}$ and $M_{x,\mathrm{B}}$. The blue areas contain all data points of the input data, with the full red line as the mean value and the dashed lines as the boundaries of the 95%-quantile.

https://doi.org/10.5194/wes-2023-163
Preprint. Discussion started: 30 January 2024

eawe european academy of wind energy
Open Access WIND ENERGY SCIENCE DISCUSSIONS

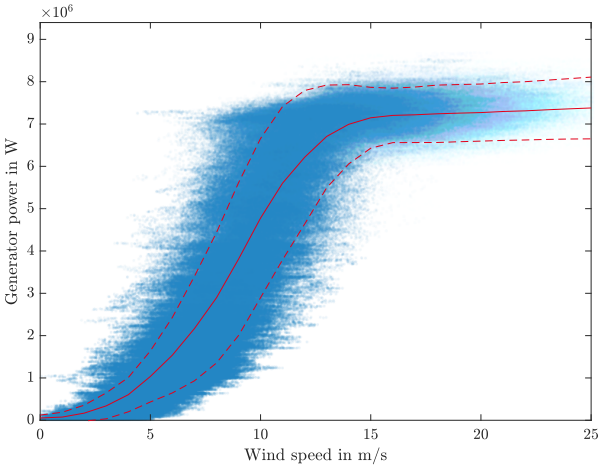

Figure 7. Generator power over wind speed from simulation data set, red line: mean value, red dashed lines: 95%-quantile

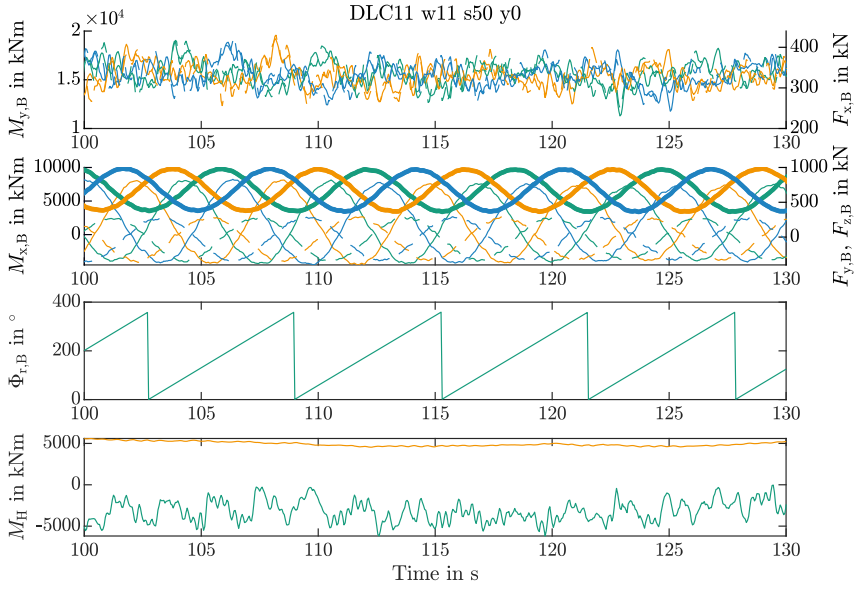

Figure 8. Time series of IWT7.5-164 at 11 m/s

In addition to the IWT7.5-164 as a reference turbine, aero-elastic time series of three commercial turbines are part of the case studies. The turbines are both onshore and offshore with rated outputs between 2 and 15 MW. The time series include power production load cases from cut in to cut out wind speed of the turbines. The finite element simulations are done with a full rotor model of one of the commercial turbines.

https://doi.org/10.5194/wes-2023-163
Preprint. Discussion started: 30 January 2024

eawe european academy of wind energy
Open Access WIND ENERGY SCIENCE DISCUSSIONS

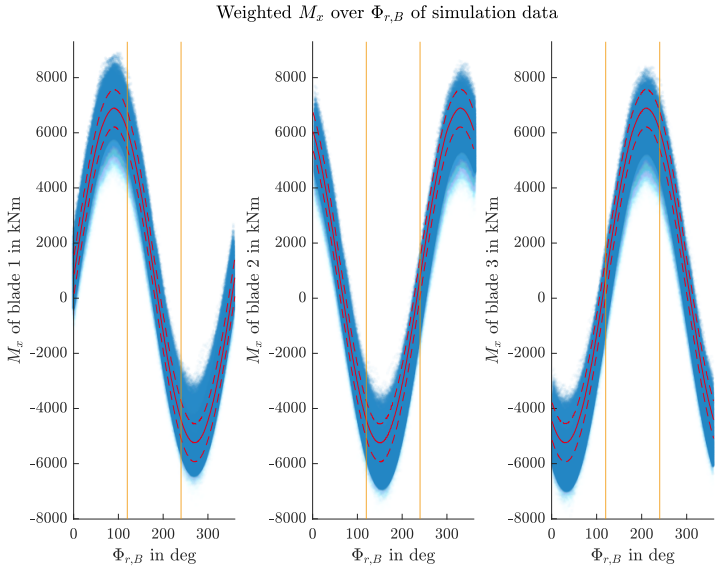

Figure 9. Weighted $M_{x,\mathrm{B}}$ of all blades over $\Phi_{\mathrm{r,B}}$, red line: mean value, red dashed lines: 95%-quantile

The scenario for the case studies is the selection of load cases for the calculation of structural fatigue of the rings of pitch bearings. It is influenced by the edgewise bending moments of all blades, as secondary blade root loads influence the stresses of the ring of the primary pitch bearing.

3.2 Finite element simulation of one rotation

To verify the central assumption of cross-influences between the individual pitch bearing loads, the first set of finite element simulations comprises one exemplary rotor rotation in twelve steps. This rotation is simulated with a full and a one-third rotor model.

Stress cycles in the outer ring drive its structural fatigue. Typically, these cycles have their highest amplitudes in the bore holes of the rings. Although other critical locations are possible, this study evaluates the tangential stresses in bore holes of the outer ring at distinct positions. These are on the y-axis of the pitch bearing coordinate system and experience high stress dynamics due to the edgewise loads. It is reasoned that a comparison between the normalized amplitudes will deliver similar results as at other locations of the ring. Figure 10 shows a typical stress distribution in an outer ring bore hole with higher values in red and lower values in blue. As axial location The lower side of the visualization is the hub side of the pitch bearing and usually experiences smaller deformations and stresses than the blade side.

Figure 11 shows stresses at two different positions of the circumference for a full and one-third rotor simulation. 90° is the position on the positive y-axis, and 270° the position on the negative y-axis. The axial position of the bore hole is defined as

https://doi.org/10.5194/wes-2023-163
Preprint. Discussion started: 30 January 2024

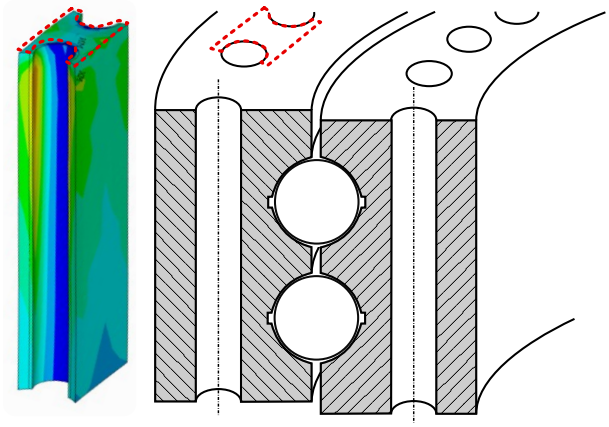

Figure 10. Visualization of tangential stresses in bore holes of outer ring (left), location in bearing (right)

195 the position of at which the maximum stress in the bore hole occurs. The results are normalized for the maximum stress at all positions.

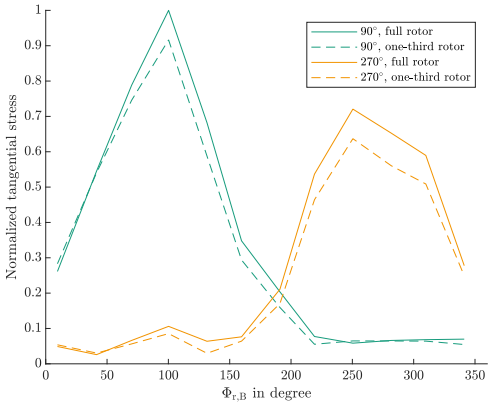

Figure 11. Normalize tangential stresses of bearing outer ring at two positions for full and one-third rotor simulations

From Figure 11, the 90°-position is identified as the more critical position for fatigue. The amplitude of the stress cycle of the one-third rotor is 9.25% lower than the one of the full rotor. This difference results in a significant difference in fatigue life

https://doi.org/10.5194/wes-2023-163
Preprint. Discussion started: 30 January 2024

eawe european academy of wind energy
Open Access WIND ENERGY SCIENCE DISCUSSIONS

and supports the initial assumption of cross-influences between the blade roots. This supports the assumed need for full rotor simulations.

The azimuthal positions of the extreme stresses in the bore holes match those of the extreme $M_{x,\mathrm{B},1}$ during the rotation. Following simulation are thus limited to these extreme values.

3.3 Bin count results

The decision criterion for the inclusion of a signal in the load case definition is the standard deviation of assumedly dependent signals, with smaller deviations being better. Due to the large number of potential dependent signals a full visualization becomes impractical. Therefore, the tables below present the standard deviations of $M_{x,\mathrm{B},2}$ and $M_{y,\mathrm{B},2}$ as representative signals. All values are normalized to the maximum value of $M_{\mathrm{y,B},1}$ and also given as percentage of the standard deviation of the signal in the full data set. The edgewise bending moments are primarily influenced by gravitational forces and thus depend on the blade's azimuth angle. The initial bin count utilizes this azimuth angle. Other potential independent signals include pitch angle, flapwise and edgewise blade bending moments and rotor moments. For the following analysis, we exclude the rotor moment about the vertical axis, $M_{\mathrm{z,H}}$, as it remains approximately constant.

Table 3 contains results for bin counts involving a single signal. With the exception of $\Phi_{\mathrm{r,B}}$ and $M_{x,\mathrm{B},1}$ as independent signals and $M_{x,\mathrm{B},2}$ as the dependent signal, increasing the number of bins did not lead to a reduction in the standard deviation of the dependent signals. Notably, $\Phi_{\mathrm{r,B}}$ significantly outperforms $M_{x,\mathrm{B},1}$ in this regard and reduces the standard deviation of $M_{x,\mathrm{B},2}$ by 86.4% in comparison to the unprocessed data set. It is also worth noting that no discernible relationship could be established between the flapwise bending moments of blade two and any of the signals selected for bin counting. For the following tests with combined bin counts, the number of 16 bins for $\Phi_{\mathrm{r,B}}$ is kept constant and $M_{x,\mathrm{B},1}$ is omitted.

Table 3. Singular bin count results

Independent signals	**Convergence bins** $M_{x,\mathrm{B},2}$	**STD** $M_{x,\mathrm{B},2}$ norm.	**STD** $M_{x,\mathrm{B},2}$ reduction	**Convergence bins** $M_{y,\mathrm{B},2}$	**STD** $M_{y,\mathrm{B},2}$ norm.	**STD** $M_{y,\mathrm{B},2}$ reduction
$\Phi_{\mathrm{r,B}}$	16	0.024	86.4%	1*	0.082	0%
$M_{x,\mathrm{B},1}$	4	0.147	16.9%	1*	0.082	0%
$M_{\mathrm{y,B},1}$	1*	0.177	0%	1*	0.082	0%
θ_1	1*	0.177	0%	1*	0.082	0%
$M_{\mathrm{y,H}}$	1*	0.177	0%	1*	0.082	0%

* no significant reduction of standard deviations with more bins

Table 4 contains results for combined bin counts, each employing 16 bins for the blade's azimuth angle as the first bin count. Interestingly, neither the pitch angle nor the out-of-plane rotor moment contributed to improving the results. However, when the flapwise and edgewise bending moments were introduced in addition to the azimuth angle, there was a noticeable reduction in the standard deviations of the selected dependent signals.

https://doi.org/10.5194/wes-2023-163
Preprint. Discussion started: 30 January 2024

eawe european academy of wind energy
Open Access WIND ENERGY SCIENCE DISCUSSIONS

Either of the moments had positive effects, with more pronounced effects when the dependent bending moments were in the same direction. For instance, binning the flapwise bending moment reduced the deviation of the flapwise moments at blade two more effectively with 32.9% than the binning of edgewise moments, which lead to a reduction by 9.8%.

Table 4. Combined bin count results with 16 bins for $\Phi_{\mathrm{r,B}}$

Independent signals	**Convergence bins** $M_{x,\mathrm{B},2}$	**STD** $M_{x,\mathrm{B},2}$ norm.	**STD** $M_{x,\mathrm{B},2}$ reduction	**Convergence bins** $M_{y,\mathrm{B},2}$	**STD** $M_{y,\mathrm{B},2}$ norm.	**STD** $M_{y,\mathrm{B},2}$ reduction
$\Phi_{\mathrm{r,B}}$ / $M_{x,\mathrm{B},1}$	16^{**}	0.020	88.7%	16^{**}	0.074	9.8%
$\Phi_{\mathrm{r,B}}$ / $M_{\mathrm{y,B},1}$	16^{**}	0.022	87.6%	16^{**}	0.055	32.9%
$\Phi_{\mathrm{r,B}}$ / θ_1	1^{*}	0.024	86.4%	1^{*}	0.079	3.6%
$\Phi_{\mathrm{r,B}}$ /$M_{\mathrm{y,H}}$	1^{*}	0.024	86.4%	1^{*}	0.079	3.6%

* no significant reduction of standard deviations with more bins
** small, but notable improvements with increasing bins

Table 5 shows results for stacked bin counts for three independent signals. Only those signal combinations that improved results in comparison to individual counts are considered. As 16 times 16 bins result in 256 bins from the combinations of $\Phi_{\mathrm{r,B}}$ and $M_{\mathrm{y,B},1}$, this evaluation is limited to eight bins as a maximum for the third signal with an eye on the overall target of less than 2000 simulations. The introduction of the pitch angle or the edgewise bending moment did not yield any significant improvements to the deviations. However, the introduction of the rotor moment $M_{\mathrm{y,H}}$ managed to reduce the standard deviation of $M_{\mathrm{y,B},1}$ by approximately 1%.

Table 5. Combined bin count results with each 16 bins for $\Phi_{\mathrm{r,B}}$ and $M_{\mathrm{y,B},1}$

Independent signals	**Convergence bins** $M_{x,\mathrm{B},2}$	**STD** $M_{x,\mathrm{B},2}$ norm.	**STD** $M_{x,\mathrm{B},2}$ reduction	**Convergence bins** $M_{y,\mathrm{B},2}$	**STD** $M_{y,\mathrm{B},2}$ norm.	**STD** $M_{y,\mathrm{B},2}$ reduction
$\Phi_{\mathrm{r,B}}$ / $M_{\mathrm{y,B},1}$ / $M_{x,\mathrm{B},1}$	1^{*}	0.020	88.7%	1^{*}	0.055	32.9%
$\Phi_{\mathrm{r,B}}$ / $M_{\mathrm{y,B},1}$ / θ_1	1^{*}	0.022	87.6%	1^{*}	0.055	32.9%
$\Phi_{\mathrm{r,B}}$ / $M_{\mathrm{y,B},1}$ / $M_{\mathrm{y,H}}$	1^{*}	0.021	88.1%	8^{**}	0.046	43.9%

* no significant reduction of standard deviations with more bins
** small, but notable improvements with increasing bins

The stacked bin count using $\Phi_{\mathrm{r,B}}$ and $M_{\mathrm{y,B},1}$ has shown promising results. Given that the selection of 16 bins for $\Phi_{\mathrm{r,B}}$ bases on its individual bin count, there is potential to explore bin reduction within the combined bin count, as presented in Table 6. The number of $\Phi_{\mathrm{r,B}}$ bins has a larger effect on the deviations of any $M_{x,\mathrm{B}}$ than on the $M_{y,\mathrm{B}}$ deviations. Conversely, the number of bins for $M_{\mathrm{y,B},1}$ has a more pronounced influence on the deviations of other $M_{y,\mathrm{B}}$ signals. Reducing the number of bins within the examined ranges consistently leads to noticeable changes in the deviations. This means the number of bins

https://doi.org/10.5194/wes-2023-163
Preprint. Discussion started: 30 January 2024

eawe european academy of wind energy
Open Access WIND ENERGY SCIENCE DISCUSSIONS

of any individual signal in the combined bin count cannot be reduced in comparison to bin counts with single signals without negative influences on the results.

Table 6. Combined bin count results with varying bins for $\Phi_{\mathrm{r,B}}$ and $M_{\mathrm{y,B,1}}$

Bins $\Phi_{\mathrm{r,B}}$	**Bins** $M_{\mathrm{y,B,1}}$	**STD** $M_{x,\mathrm{B},1}$	**STD** $M_{x,\mathrm{B},2}$	**STD** $M_{x,\mathrm{B},3}$	**STD** $M_{y,\mathrm{B},2}$	**STD** $M_{y,\mathrm{B},3}$
16	16	0.020	0.022	0.022	0.055	0.055
16	8	0.021	0.023	0.023	0.060	0.060
8	16	0.037	0.039	0.039	0.055	0.055
8	8	0.038	0.039	0.039	0.060	0.060
4	16	0.076	0.070	0.070	0.057	0.057
4	8	0.076	0.070	0.070	0.061	0.061
4	4	0.077	0.071	0.071	0.068	0.068

The each 16 bins for $\Phi_{\mathrm{r,B}}$ and $M_{\mathrm{y,B,1}}$ are then applied to time series of three commercial turbines. Table 7 gives the results in relative reduction of standard deviations after the bin counts. The first result line contains the IWT7.5-164 results as a reference.

Table 7. Bin count results with each 16 bins for $\Phi_{\mathrm{r,B}}$ and $M_{\mathrm{y,B,1}}$ and commercial turbines

Turbine	**STD** $M_{x,\mathrm{B},1}$ reduction	**STD** $M_{x,\mathrm{B},2}$ reduction	**STD** $M_{x,\mathrm{B},3}$ reduction	**STD** $M_{y,\mathrm{B},2}$ reduction	**STD** $M_{y,\mathrm{B},3}$ reduction
IWT	88.7%	87.6%	87.6%	32.9%	32.9%
1	86.9%	86.4%	86.4%	26.8%	26.5%
2	87.6%	87.1%	87.1%	37.7%	37.4%
3	82.5%	82.0%	81.8%	49.8%	49.8%

3.4 Verification by finite element simulations

To understand the influence of variations introduced by the bin counting, the following comparisons repeat the simulations with the full rotor model described in Section 3.2. As the extreme stresses in the bore hole at 90° coincide with the extreme $M_{x,\mathrm{B},1}$, they omit steps in between. The difference between the stresses obtained at minimum and maximum $M_{x,\mathrm{B},1}$ is the stress amplitude of the rotation. Table 8 lists the influence of variations of all $M_{x,\mathrm{B}}$ and only secondary $M_{x,\mathrm{B}}$ on this stress amplitude at the 90°-position.

The variations of all $M_{x,\mathrm{B}}$ by the standard deviations lead to significant changes in the stress amplitude. The load case definition thus cannot rely only on $\Phi_{\mathrm{r,B}}$ and $M_{x,\mathrm{B},1}$. Hence, $M_{x,\mathrm{B},1}$ is introduced as a further parameter of the load case

https://doi.org/10.5194/wes-2023-163
Preprint. Discussion started: 30 January 2024

eawe european academy of wind energy
Open Access WIND ENERGY SCIENCE DISCUSSIONS

definition. This leads to far better results in comparison to the two-dimensional load case definition and surpasses the results of a one-third model as well.

Table 8. Variation with standard deviations

Description of load case variant	Amplitude deviation to full rotor
All $M_{x,\mathrm{B}}$ plus standard deviation from bin counting	7.19%
All $M_{x,\mathrm{B}}$ minus standard deviation from bin counting	-6.74%
$M_{x,\mathrm{B},2}$ and $M_{x,\mathrm{B},3}$ plus standard deviation from bin counting	-0.57%
$M_{x,\mathrm{B},2}$ and $M_{x,\mathrm{B},3}$ minus standard deviation from bin counting	-0.26%

3.5 Calculation of missing blade azimuth angle

As the blade's azimuth angle is the single most important signal for the bin counting and might be missing from the input data set, this section covers the use of a calculated $\Phi_{\mathrm{r,B}}$ as described in Section 2.3.

For the entire data set of the IWT7.5-164 reference turbine, $\Phi_{\mathrm{r,B}}$ was computed. Figure 12 visualizes exemplary results. The original values are shown as dashed red line and the calculated values as blue line. To provide a reference, the figure also includes $M_{x,\mathrm{B},1}$. The zero position for the calculated azimuth angle was aligned to the local maxima of the derivative of the filtered $M_{x,\mathrm{B},1}$. A slight phase shift is observable, attributed to the fact that $M_{x,\mathrm{B},1}$ is not precisely zero at the upper dead point of the blade's circular motion. This load case at mean wind speed of $19\,\mathrm{m/s}$ showed a comparatively pronounced frequency content above 1p in $M_{x,\mathrm{B},1}$ and is displayed to show the robustness of the algorithm.

To assess the validity of the calculated azimuth angle signal $\Phi_{\mathrm{r,B,calc}}$ for bin counting purposes, Table 9 reproduces some of the bin combinations of Table 6 with the calculated azimuth angle. The results in Table 9 exhibit only very minor differences when compared to those in Table 6.

Table 9. Combined bin count results with varying bins for $\Phi_{\mathrm{r,B,calc}}$ and $M_{\mathrm{y,B},1}$

Bins $\Phi_{\mathrm{r,B}}$	**Bins** $M_{\mathrm{y,B},1}$	**STD** $M_{x,\mathrm{B},1}$	**STD** $M_{x,\mathrm{B},2}$	**STD** $M_{x,\mathrm{B},3}$	**STD** $M_{y,\mathrm{B},2}$	**STD** $M_{y,\mathrm{B},3}$
16	16	0.021	0.023	0.023	0.054	0.054
16	8	0.021	0.023	0.023	0.060	0.060
16	4	0.022	0.024	0.024	0.067	0.067

3.6 Selection of load cases

Table 10 lists the selected signals and the respective bins, resulting in a total of 16384 load cases. 27 out of the 256 combinations from the stacked bin count involving azimuth angle and flapwise bending moment yielded zero samples. These instances

https://doi.org/10.5194/wes-2023-163
Preprint. Discussion started: 30 January 2024

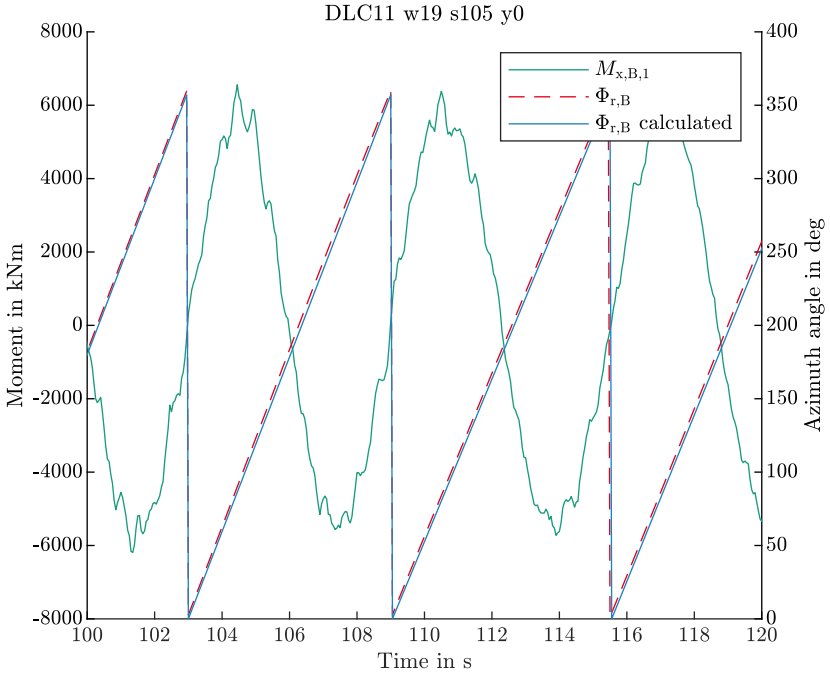

Figure 12. Exemplary comparison of original and calculated $\Phi_{r,B}$

occurred exclusively at the edges of the bin ranges. As such, omitting these cases carries no adverse consequences, effectively reducing the overall required load cases to 14656.

Table 10. Preliminary load case selection for pitch bearing ring and hub fatigue simulations

Signal	Criteria	Bins	Remarks
$\Phi_{r,B}$	Allows definition of $M_{x,B,2}$, $M_{x,B,3}$ and all $F_{y,B}$ and $F_{z,B}$	16	Finer resolution does not improve deviations significantly
$M_{x,B,1}$	Defines stress state for bearing locations close to y-axis	8	Sine characteristics of signal allow lower bin number than for $M_{y,B,1}$
$M_{y,B,1}$	Allows definition of all $M_{y,B}$ and $F_{x,B}$	16	Finer resolution does not improve deviations significantly
θ_1	Influences load distribution in the bearing	8	Taken from (Menck et al., 2020)

Further on, the selection of 8 distinct pitch angles is derived from previous work and has not yet been validated for the purpose of the structural fatigue calculations. Based on just one pitch angle for the simulation the load cases reduce to 1832.

https://doi.org/10.5194/wes-2023-163
Preprint. Discussion started: 30 January 2024

eawe european academy of wind energy
Open Access WIND ENERGY SCIENCE DISCUSSIONS

With the computational resources available for this work, this number is still too high for reasonable times. Further reductions for the calculations of pitch bearing ring fatigue is possible if load cases in between extreme values of $M_{x,\mathrm{B},1}$ and $M_{\mathrm{y},\mathrm{B},1}$ are omitted and the results interpolated between the remaining values. This keeps the important simulation load cases that give stress amplitudes. Table11 lists the resulting number of cases which result in a total of 384 simulations and are in the range of simulations done in Menck et al. (2020).

Table 11. Final load case selection for pitch bearing ring fatigue simulations

Signal	Criteria	Bins	Remarks
$\Phi_{\mathrm{r},\mathrm{B}}$	Allows definition of $M_{x,\mathrm{B},2}$, $M_{x,\mathrm{B},3}$ and all $F_{y,\mathrm{B}}$ and $F_{z,\mathrm{B}}$	8	Omit four bins at 0° and four bins at 180°
$M_{x,\mathrm{B},1}$	Defines stress state for bearing locations close to y-axis	6	Omit two bins at center of value range
$M_{\mathrm{y},\mathrm{B},1}$	Allows definition of all $M_{y,\mathrm{B}}$ and $F_{x,\mathrm{B}}$	8	Omit eight bins in center of value range
θ_1		1	Do few additional simulation to evaluate worst influence

4 Discussion and conclusions

The present work covers the selection of load cases for finite element simulation of wind turbine rotors. Such simulations are used for the design of pitch bearings and hubs. Given the substantial complexity and size of the finite element models, conducting a large number of simulations within a reasonable timeframe becomes challenging. Detailed fatigue calculations, however, necessitate such a large number of simulations to establish the nonlinear relationships between external loads and internal stresses or contact pressures.

To address this challenge, the present study aims to uncover relations in between individual loads of the rotor blade roots and loads and rotational position of the hub center. This is accomplished through the use of stacked bin counts and an evaluation of standard deviations of other signals within these bins.

In addition to the blade root load signals used in approaches documented in the literature, this study incorporates the blade azimuth angle and the rotor out-of-plane moments for the evaluations. Novel methods for deriving these signals from the blade roots' loads are proposed. The algorithm introduced for calculating the blade azimuth angle has undergone successful testing.

The inclusion of the blade's azimuth angle, denoted as $\Phi_{\mathrm{r},\mathrm{B}}$, renders promising outcomes by narrowing down the range of values of the edgewise bending moments. When combined with $M_{\mathrm{y},\mathrm{B},1}$ and $M_{x,\mathrm{B},1}$ this integration significantly reduces deviations across all load components in comparison to the original data set and was proven to result in similar stress cycle amplitudes as the simulation of a full rotor with load cases based on time series. The maximum deviation of stress amplitudes in the case study was 0.57%. To result in a reasonable number of simulations, however, it was necessary to remove bins which result in stress values at the center of the value range. This made the approach more similar to the rainflow-count based one in (Becker and Jorgensen, 2023).

https://doi.org/10.5194/wes-2023-163
Preprint. Discussion started: 30 January 2024

Introducing the out-of-plane rotor moment proves to be beneficial when combined with the blade azimuth angle and flapwise bending moment. However, it's important to note that this addition brings an extra dimension to the parameter space of the simulation load cases, resulting in higher computational costs.

Based on the findings of the bin counting and exemplary finite element simulations, the blade azimuth angle and the bending moments are chosen for the load case definition of full rotor simulations.

The present work verified this approach for one exemplary turbine and the use case of pitch bearing ring fatigue.

Data availability. The time series data from aero-elastic simulation are available from the authors upon request.

Author contributions. MS: Idea, data analysis, bin counting, writing
FS: Finite element simulations, writing, review

Competing interests. The authors declare there are no competing interests.

Acknowledgements. This work was carried out within the project BALTIC. The funding by the BMWK, Federal Ministry for Economic Affairs and Climate Action (Federal Republic of Germany), under grant number 03EE3019A, is kindly acknowledged. Niklas Requate's time series are the base of the IWT case study in this paper and the authors thank him for the permission to use them. Arne Bartschat suggested to use the rotor tilting moments as signals for the bin counts.

https://doi.org/10.5194/wes-2023-163
Preprint. Discussion started: 30 January 2024

eawe european academy of wind energy
Open Access WIND ENERGY SCIENCE DISCUSSIONS

References

Becker, D. and Jorgensen, T.: Multi MW Blade Bearing Applications – Advanced Blade Bearing Design Process and Pitch Bearing Module Development Trends, 2023.

Becker, D., Gockel, A., Handreck, T., Lüneburg, B., Netz, T., and Vollmer, G.: State-of-the-art design process for pitch bearing applications of multi-MW wind turbine generators, in: Conference for Wind Power Drives, pp. 17–, Aachen, 2017.

Burton, T., Jenkins, N., Sharpe, D., and Bossanyi, E.: Wind Energy Handbook, Wiley, Chichester and New York, 2nd ed edn., 2011.

Chen, G. and Wen, J.: Load Performance of Large-Scale Rolling Bearings With Supporting Structure in Wind Turbines, Journal of Tribology, 2012, 2012.

FKM: Analytical Strength Assessment of Components, 2012.

Graßmann, M., Schleich, F., and Stammler, M.: Validation of a finite-element model of a wind turbine blade bearing, Finite Elements in Analysis and Design, 221, 103 957, https://doi.org/10.1016/j.finel.2023.103957, 2023.

Hau, E.: Windkraftanlagen: Grundlagen. Technik. Einsatz. Wirtschaftlichkeit, Springer Berlin Heidelberg, Berlin, Heidelberg, sixth edn., https://ebookcentral.proquest.com/lib/gbv/detail.action?docID=4818780, 2017.

ISO: Rolling bearings — Damage and failures — Terms, characteristics and causes, 2017.

Menck, O., Stammler, M., and Schleich, F.: Fatigue lifetime calculation of wind turbine blade bearings considering blade-dependent load distribution, Wind Energy Science, 5, 1743–1754, https://doi.org/10.5194/wes-5-1743-2020, 2020.

Requate, N., Wiens, M., and Meyer, T.: A Structured Wind Turbine Controller Evaluation Process Embedded into the V-Model for System Development, Journal of Physics: Conference Series, 1618, 022 045, https://doi.org/10.1088/1742-6596/1618/2/022045, 2020.

Sevinc, A., Rosemeier, M., Bätge, M., Braun, R., Meng, F., Shan, M., Horte, D., Balzani, C., and Reuter, A.: IWES Wind Turbine IWT-7.5-164, Hannover, 2014.

Stammler, M.: Endurance Test Strategies for Pitch Bearings of Wind Turbines, Fraunhofer Verlag, Stuttgart, 2020.

Stammler, M., Baust, S., Reuter, A., and Poll, G.: Load distribution in a roller-type rotor blade bearing, Journal of Physics: Conference Series, 1037, https://doi.org/10.1088/1742-6596/1037/4/042016, 2018.

Stammler, M., Thomas, P., Reuter, A., Schwack, F., and Poll, G.: Effect of load reduction mechanisms on loads and blade bearing movements of wind turbines, Wind Energy, 6, 119, https://doi.org/10.1002/we.2428, 2019.